



Gravitational instabilities triggered by fluid overpressure and downslope incision – Insights from analytical and analogue modelling

Aurélien Lacoste^{a,*}, Bruno C. Vendeville^b, Régis Mourgues^a, Lies Loncke^c, Maxime Lebacqz^b

^a LGPN, UMR 6112, Université du Maine, Avenue Olivier Messiaen, 72085 Le Mans Cedex 09, France

^b UMR 8217 Géosystèmes, Université de Lille 1, Cité scientifique, Bâtiment SN5, 59655 Villeneuve d'Ascq, France

^c Université de Perpignan Via Domitia, Laboratoire IMAGES, 52 avenue Paul Alduy, 66800 Perpignan, France

ARTICLE INFO

Article history:

Received 19 December 2011

Received in revised form

21 May 2012

Accepted 25 May 2012

Available online 6 June 2012

Keywords:

Gravitational instabilities

Fluid overpressure

Analytical modelling

Analogue modelling

ABSTRACT

Fluid overpressure at the base of low-permeability strata reduces effective stress, allowing for gravitational sliding of the overlying cover. The force driving sliding is the slope-parallel component of the weight of the cover, whereas the resisting forces are the friction at the base of the cover and the buttressing resistance to shortening, which can be critically reduced by incision at the base of the slope. We developed an analytical model and undertook a series of analogue experiments to better understand the evolution of a sedimentary cover sliding above a low-permeability layer subjected to fluid overpressure. Where a downslope buttress was present, the sliding sheet length decreased with increasing pore-fluid pressure. In the absence of such buttress, the slide's length increased exponentially with increasing pore-fluid pressure. Another important difference dealt with geometry and kinematics. Buttressed slides consisted of one large slope-parallel mass rigidly translated and bounded by downslope thrusts and upslope normal faults. With increasing pore-fluid pressure, the contractional structures propagated upslope. By contrast, non-buttressed slides showed intense strain: deformation started with normal faults forming near the incision, then propagating upslope throughout the slide's evolution.

© 2012 Elsevier Ltd. All rights reserved.

1. Introduction

Mass movements are a major erosional process along both passive and active margins. The onset of gravitational instabilities is the result of the effect of preparatory factors, such as the lithology of the décollement layer and of the cover, coupled with external predisposing factors reducing the forces resisting downward motion, such as seismic activity (Keefer, 1984), heavy rainfall (Chen et al., 2006) or fluid overpressure (Mourgues et al., 2009). In particular, these factors cause the effective stress of weak layers, such as shale, to decrease. Therefore, these layers may act as décollement layers for the overlying cover.

Terzaghi (1923) and Hubbert and Rubey (1959) have demonstrated that the effective rock stress of low-permeability layers, hence the frictional force between such layers and the overlying cover, can be critically reduced in the presence of fluid overpressure. Overpressures are responsible for promoting gravitational submarine slides, as in the Amazon fan (Cobbald et al., 2004; Mourgues et al., 2009), the Niger delta (Weber and Daukora, 1975;

Hooper et al., 2002), or the Champion delta (Van Rensbergen and Morley, 2000), and avalanches (e.g., the Storegga slide, Norway, ~3000 km³, Hafidason et al., 2004), as well as large onshore mass movements (Waitawhiti landslides, New Zealand, 111.10⁶ m³, Lacoste et al., 2009).

Besides, sliding along a detachment plane can be facilitated in the case of the absence of force resisting shortening at the base of the slope. Such a force can be decreased, and even entirely eliminated, by downslope incision, therefore leading to landsliding. However, the triggering of gravitational instability when the downslope buttress is removed requires an incision that is deep enough, cutting the cover all the way down to the mechanically weak layers (e.g., swelling clays, Azañon et al., 2005; overpressured shale, Lacoste et al., 2011).

Mourgues and Cobbald (2006) and Mourgues et al. (2009) have conducted analogue sandbox modelling of sliding above overpressured shale, in which compressed air was applied at the base of a low-permeability layer, therefore promoting sliding. In these models having a downslope buttress, sliding can occur only if the driving force can overcome the buttressing resisting force downslope, i.e., if the slide reaches a minimum required length (Mourgues and Cobbald, 2006; Mourgues et al., 2009). These authors observed that, in the presence of a resisting force at the

* Corresponding author. Tel.: +33 2 43832653; fax: +33 2 43833795.
E-mail address: aurelacoste@gmail.com (A. Lacoste).

base of the slope, the sliding mass comprised three distinct domains: (1) an extensional domain upslope, (2) a non-deformed slab at mid-slope and (3) a contractional domain downslope (Fig. 1A). Mourgues and Cobbold (2006) also showed that the cover deformation was greater (a greater number of normal faults and thrusts initiated in the upslope and downslope parts of the model, respectively) where the value of the basal slope angle was higher. The downward displacement of the non-deformed slab also increased with the basal slope angle increasing.

Lacoste et al. (2011) have investigated experimentally the influence of the permanent removal of the downslope buttress on the initiation, structure and evolution of such gravity-driven instabilities. They showed that, in models subjected to constant valley incision, gravitational collapse and normal faulting propagated retrogressively from the valley flanks to the upslope domain (Fig. 1B). The number of faults, as well as the area affected by deformation, increased with increasing air pressure. The deformed area also greatly increased with increasing basal slopes.

In this article, we present, on the basis of the work by Mourgues and Cobbold (2006), a 2-D analytical model of gravity sliding of a sedimentary cover on a plane subjected to fluid overpressure. We calculate the forces applied to the system and determine the minimum slide length required for sliding to occur, under different boundary conditions: (1) in the presence and (2) in the absence of a downslope buttress. We also document two series of experimental

models that we conducted to confirm our analytical predictions. Finally, we discuss the discrepancies between analytical predictions and experimental data to determine more precisely the influence of the absence and the presence of a downslope buttress on the structural style.

2. Analytical expression of the sliding sheet length

To outline the morphological evolution of masses sliding above a planar substratum subjected to pore-fluid overpressure, we built a mechanical model based on the equilibrium of forces and assumptions on the effective stresses.

2.1. Infinite slope model

It is first convenient to consider the simplistic case of an infinite slope (Terzaghi, 1950; Hubbert and Rubey, 1959; Lambe and Whitman, 1969; Crans et al., 1980; Mandl and Crans, 1981; Mello and Pratson, 1999). The equation of equilibrium of total stresses in the sediments subjected to gravity is:

$$\nabla\sigma = \rho_b g \quad (1)$$

where σ is the total stress tensor, g is the gravity and ρ_b the bulk density. The presence of fluids in the porous medium implies that a part of the total stresses is supported by the fluid phase. Terzaghi

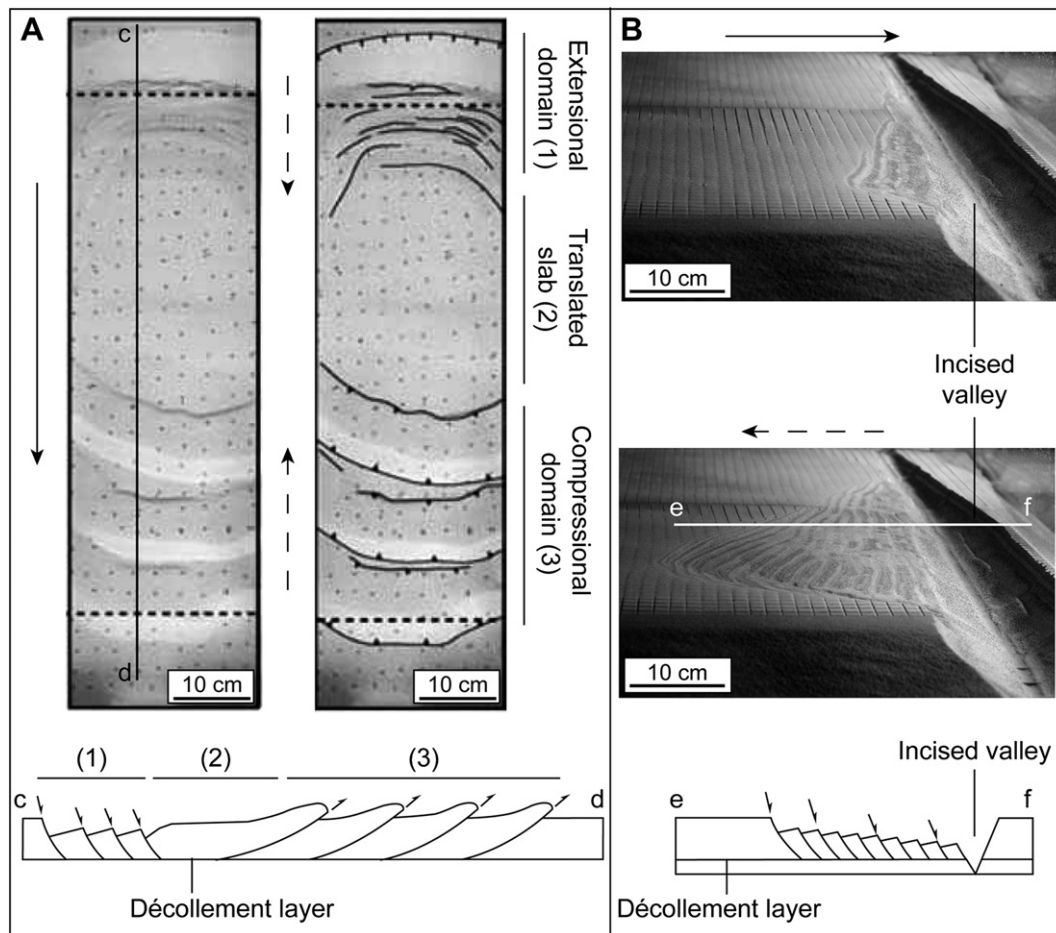


Fig. 1. Analogue sandbox modelling of sliding above an overpressured low-permeability layer. (A) Top: Overhead photograph (left) and line-drawing (right) of a model having a downslope buttress (Mourgues and Cobbold, 2006). Bottom: Schematic cross section. (B) Side photographs of the initial (top) and last (centre) stages of a model with a downslope incision (Lacoste et al., 2011). Bottom: Schematic cross section. Solid arrows indicate the sense of sliding. Dashed arrows show the sense of propagation of the deformation.

(1923) defined the effective stress tensor σ' as the sole parameter controlling the deformation of a porous media:

$$\sigma' = \sigma - P_f Id \quad (2)$$

with P_f the pore pressure and Id the identity matrix. Expressed in terms of effective stresses, Eq. (1) becomes:

$$\nabla \sigma' = \rho_b g - \nabla P_f = \rho_b g - \rho_w g - \nabla P_{ov} = \rho_e g - \nabla P_{ov} \quad (3)$$

with ρ_w the density of water. $\rho_w g$ is the hydrostatic part of the fluid pressure gradient ∇P_f . $\rho_w g$ acts on the solid matrix as a buoyancy force (body force) equivalent to the Archimedes force (Dahlen, 1990; Mourgues and Cobbold, 2003). The effective weight of the sediments then becomes the buoyant weight $\rho_e g = \rho_b g - \rho_w g$. ∇P_{ov} is the non-hydrostatic part of ∇P_f , also called gradient of fluid overpressure. This gradient induces a seepage force $-\nabla P_{ov}$ to the system. This force is not inevitably vertical and therefore may contribute to slope instability. With references axes (x , z) being respectively parallel and perpendicular to the slope α , Eq. (3) becomes:

$$\partial \sigma'_{xx} / \partial x + \partial \sigma'_{xz} / \partial z = \rho_e g \sin \alpha + \partial P_{ov} / \partial x \quad (4a)$$

$$\partial \sigma'_{xz} / \partial x + \partial \sigma'_{zz} / \partial z = \rho_e g \cos \alpha + \partial P_{ov} / \partial z \quad (4b)$$

In the infinite slope model, the assumption is made that the slope is long enough so that longitudinal stress gradients are negligible: $\partial \sigma'_{xx} / \partial x = \partial \sigma'_{xz} / \partial x = 0$. The gradient of fluid overpressure is assumed to be perpendicular to the slope. Mandl and Crans (1981) justified this approximation on the grounds that compaction is invariant along the slope and that the principal axes of the permeability tensor are approximately parallel and perpendicular to the free surface. In such analysis, we define the generalized pore-fluid overpressure ratio, modified from Hubbert and Rubey (1959):

$$\lambda = P_{ov} / \rho_e g z \cos \alpha \quad (5)$$

with P_{ov} the pore-fluid pressure at depth z , ρ_e the effective density of the sliding cover ($\rho_e = \rho_b - \rho_w$) and α the basal slope angle.

We consider in this study the case of a non-cohesive system. Assuming that sediments obey a Mohr–Coulomb criterion of deformation, gliding occurs when the shear stress on a plane parallel to the slope reaches the yield stress, following the Coulomb law:

$$\sigma'_{xz} = \tau = \mu \sigma'_{zz} \quad (6)$$

with τ the shear stress at yield, μ the coefficient of internal friction. On the upper surface of the sediments ($z = 0$), $\sigma'_{xz} = 0$. Combining Eqs. (4)–(6) therefore leads to the condition required for sliding of the cohesionless cover (Hubbert and Rubey, 1959):

$$\tan \alpha = (1 - \lambda) \tan \phi \quad (7)$$

with ϕ the angle of friction. It is here important to underline that the hydrostatic pore pressure has no effect on the stability

of a submarine slope. Indeed, under hydrostatic conditions, the stability of a submarine slope is similar to that of a dry emerged slope. In stratified sediments, the pressure gradient varies from one layer to another in response to changes in permeability. We will assume thereafter a sedimentary cover having a constant coefficient of fluid pressure λ and an angle of friction ϕ . At the base of this cover, the coefficient of fluid pressure and the coefficient of friction have specific values λ_b and μ_b , respectively (Davis et al., 1983). For a detachment to occur at the base of the cover:

$$\mu_b (1 - \lambda_b) \leq \mu (1 - \lambda) \quad (8)$$

2.1.2. Length of a frontally confined sliding sheet

In the infinite slope model, stress gradient is not parallel to the slope. As a consequence, as soon as condition (8) is satisfied, the cover may slide. However, in natural systems, lateral variations of pore pressure and mechanical parameters may induce a resistance at the toe (Fig. 2A).

When a detachment appears, part of the weight of the cover is transferred from the base to the toe. Sliding occurs when the transferred weight reaches values high enough to overcome the distal buttress resisting force and initiate thrust faults, i.e. when the sliding mass reaches a certain length. Lambe and Whitman (1969), Mandl (1988) and Mourgues and Cobbold (2006) showed that the minimal length necessary for sliding to occur can be determined by writing the balance between forces driving downward motion of the sedimentary cover and forces resisting this motion. Lambe and Whitman (1969) demonstrated that the following force systems could be used when evaluating the stability of a wedge:

- Total weight, boundary pore pressures and boundary effective stresses,
- Buoyant weight, seepage force and boundary effective stresses.

These two approaches are strictly equivalent, and we chose to use the latter in our study.

In the case of an infinite slope, the main driving force derives from the slope-parallel component of the weight (hereafter denoted as F_w) and the resisting force arises from frictional resistance (F_b) along the sliding plane. When considering sliding sheets having a finite length (Fig. 2A), additional forces must be introduced: the resistance on the lower edge (F_{σ}^{toe}) and the result of stresses on the upper edge (F_{σ}^{ext}) (Terzaghi, 1959). The driving force F_{σ}^{ext} , generated by the thrust of the mass upslope the upper edge of the sliding cover, and the resisting force F_{σ}^{toe} , induced by the presence of a downslope buttress, correspond to Rankine active and passive states, respectively (Lambe and Whitman, 1969). When writing the balance of forces applied to a buttressed system (see Appendix for further details), we obtain the length L of the sliding sheet:

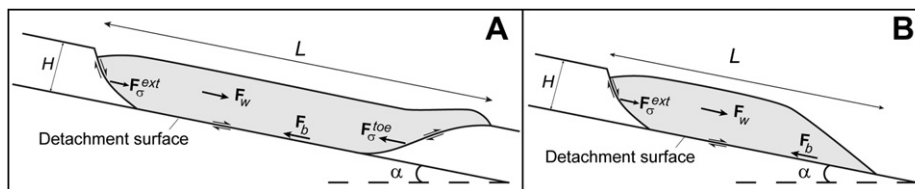


Fig. 2. Stresses and forces applied in a buttressed model (A) and an incised model (B). F_w is the driving force induced by the weight of the model, F_b is the basal frictional resisting force, F_{σ}^{ext} and F_{σ}^{toe} are the forces exerted by σ'_{xx} acting on the upper and lower edges of the system, respectively.

$$L = \frac{2(1 - \lambda)\mu\sqrt{1 - FS^2}}{(\tan \alpha - (1 - \lambda_b)\mu_b)\cos \phi} H \quad (9)$$

with H the cover thickness and $FS = \tan \alpha / ((1 - \lambda)\tan \phi)$

2.1.3. Length of a sliding sheet where the distal buttress is absent

Where the downslope buttress has been removed by incision, the basal detachment may intersect the bevelled surface (Fig. 2B). In such system, $F_{\sigma}^{oe} = 0$ and $F_{\sigma} = F_{\sigma}^{ext}$. Considering a cohesionless system, we obtain:

$$F_{\sigma} = F_{\sigma}^{ext} = \int_H \sigma_{xx}^{ext} dh = 0.5(1 - \lambda)\rho_e g H^2 (2Y - 1) \cos \alpha \quad (10)$$

with $Y = (1 \pm \sin \phi \sqrt{1 - FS^2}) / \cos^2 \phi$. Where the cover is cohesive, a vertical cliff may form downslope, whereas a slope having a negligible cohesion remains subjected to the critical taper conditions (Dahlen, 1984). For convenience, we will assume the wedge-like downslope part of the cover to have a stable surface slope and to slide rigidly. In comparison with the buttressed model, the seepage force in this case has an x -component that must be added to the balance of forces. We obtain the sliding sheet length by writing the balance of forces applied to a non-buttressed system (see Appendix for details):

$$L = 0.5 \left(\frac{(1 - \lambda)(2Y - 1) + \lambda}{\mu_b(1 - \lambda_b) - \tan \alpha} - \frac{1}{\tan \beta} \right) H \quad (11)$$

2.2. Analytical results

In this section, we describe the evolution of the sliding sheet length at yield, depending on the boundary conditions. Mourgues and Cobbold (2006) and Lacoste et al. (2011) showed that the evolution of the deformation greatly differed depending on whether or not a distal buttress was present (Fig. 1). To better understand these differences, we plotted, for both cases, the sliding sheet lengths versus the coefficient of fluid pressure λ_b (Fig. 3).

Our model confirms the observation by Mourgues and Cobbold (2006) and Mourgues et al. (2009) that a minimum length is required for the driving forces (i.e., the weight of the cover) to overcome the frictional and the downslope buttress resisting forces. This length decreases with increasing λ_b , because of the

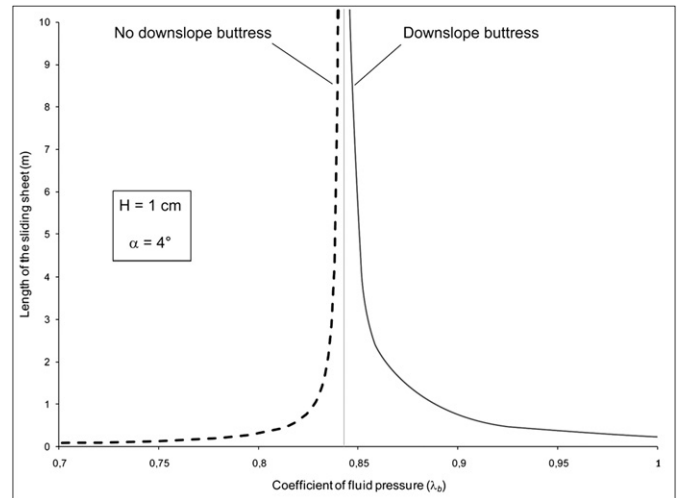


Fig. 3. Evolution of the sliding sheet length with respect to the coefficient of fluid pressure (λ_b), in the presence (bold line) or in the absence (dashed line) of a downslope buttress. The vertical asymptote corresponds to the infinite slope model.

decrease of the frictional force by fluid overpressure (Fig. 3). By contrast, the predicted sliding sheet length increases with increasing coefficient of fluid pressure (λ_b) in models having no downslope resisting force (Fig. 3). In this case, the curve also has a horizontal and a vertical asymptote (Fig. 3). The horizontal asymptote shows that short instabilities may form even where the value of λ_b is low. The vertical asymptote corresponds to values of λ_b for which the sliding sheet may reach an infinite length. This case corresponds to the infinite slope model (Mandl and Crans, 1981), in which the entire cover is predicted to slide for a given value of λ_b . This value can be determined either graphically or using Eq. (8).

We also determined the sliding sheet length evolution with respect to λ_b for different values of the basal slope angle (α) and cover thickness (H) (Fig. 4). The physical properties of the materials we used are presented in Table 1. Where a buttress is present, a greater slope (α) requires smaller values of the coefficient of fluid pressure at the base (λ_b) to trigger sliding, thus facilitating mass movement (Fig. 4A). On the contrary, where the cover is thicker, the critical fluid pressure is greater. Increases in the slope angle strongly reduces the value of λ_b required to trigger sliding (Fig. 4A), whereas variations in cover thickness has only a minor influence

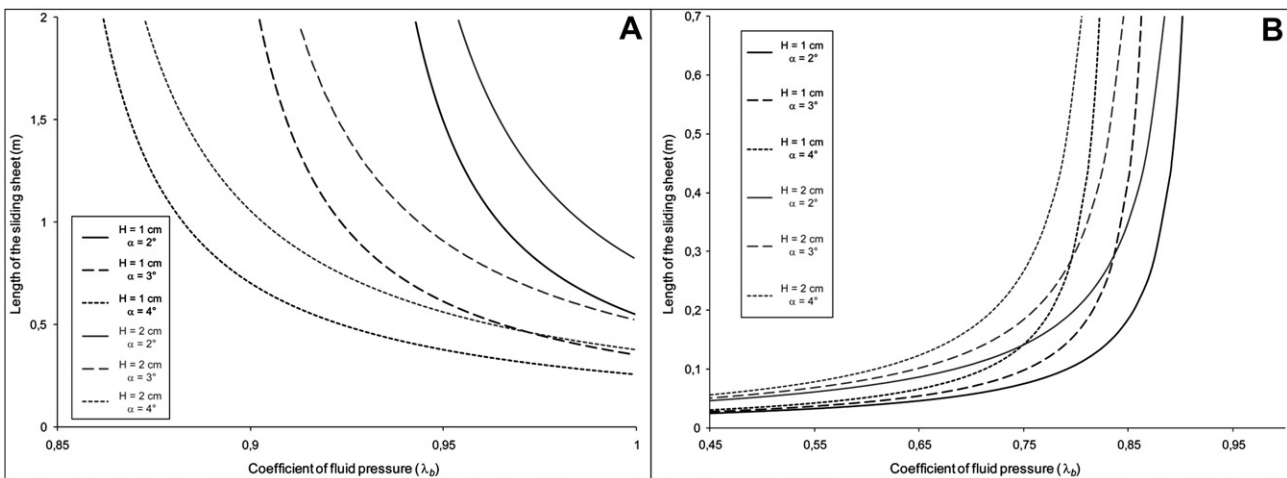


Fig. 4. Influence of the basal slope angle (α) and the cover thickness (H) on the evolution of the sliding sheet length with respect to λ_b in the presence (A) and in the absence (B) of a downslope buttress.

Table 1

Physical properties of the materials used in this study. Bulk densities and angles of internal friction were determined after Schellart (2000), Panien et al. (2006) and Yamada et al. (2006).

Material	Grain size (μm)	Bulk density (kg m^{-3})	Angle of internal friction ($^{\circ}$)	Coefficient of internal friction μ	Permeability (Darcy)	Cohesion (Pa)
Coarse sand (cover)	316	1600	34	0.67	100	0
Glass microbeads (décollement)	106	1600	24	0.44	6	0

(Fig. 4A). On the other hand, in non-buttressed models, an increase in the basal slope angle and/or in the cover thickness leads to a decrease in the fluid pressure required to trigger sliding (Fig. 4B).

3. Experimental modelling

3.1. Experimental set-up and procedure

We used the experimental set-up built by Mourgues et al. (2009). The models were constructed between two fixed lateral glass walls, on top of a sieve at the base of which compressed air was injected (Fig. 5A). The distribution of the air pressure in the models varied with the pressure applied at the model's base, and the thickness and permeability of the layers (Fig. 5B). During the experiments, the air pressure was monitored using a digital manometer (precision $\pm 0.1\%$). Our models comprised a 3 cm coarse sand (Table 1) substratum layer, overlain by a 0.5 mm low-permeability layer of glass microbeads (Table 1) layer and a coarse sand cover (Fig. 5A). Mourgues and Cobbold (2006) showed that high permeability contrasts between the décollement and the cover promote gravity sliding. Coarse sand allowed for rapid air flow, hence low air pressure, below and above the low-permeability décollement layer. We considered the cohesion of the sand and microbeads to be negligible (Table 1). Indeed, in the moisture conditions of the laboratory ($\sim 40\%$), no vertical cliff could form in these materials.

Models were 150 cm long, 60 cm large, and were built on a tilted base, with or without a downslope initial incision (Fig. 5). In both cases, we performed two series of experiments, corresponding to cover thicknesses of 1 cm and 2 cm, respectively. Each series comprised three experiments, corresponding to basal slopes ranging between 2° and 4° .

We raised the air pressure at the base until sliding of the cover occurred. For each sliding episode, we measured, on the basis of overhead photographs, the length of the sliding sheet. In the incised models, immediately after each sliding episode, we removed the slid material, to prevent the formation of a downslope buttress. In both buttressed and incised series of experiments, we then raised the air pressure again. We repeated this operation until

the whole model either deformed or exploded. The air pressure, measured continuously through the experiments, allowed us to calculate the value of the coefficient of fluid pressure λ_b for each deformation episode. We measured the pressure at the top of the homogenizing box. Nevertheless, pressure values at the base of the low-permeability layer differ because of the loss in pressure head due to the sudden flow expansion between the connecting pipes and the basal injectors (Fig. 5). We measured this head loss experimentally. Actual pressure values at the base of the model are about 70% the pressure values measured at the top of the homogenizing box (Fig. 5). Potential air spread outside the model, especially in lateral areas, may also lead to misestimating the pressures.

3.2. Experimental limitations

The experimental procedure we followed faced two major technical constraints.

- (1) The friction along the sidewalls tends to resist sliding and, because the forces driving deformation are small, can greatly influence deformation and control the 3-D morphology of faults and thrusts. Therefore, we built models that were wide compared with their thickness and we measured the sliding sheet lengths in the centre of our models, where the influence of sidewall friction was minimal. Finally, in most models, we inserted glass microbeads along the sidewalls to reduce the effective stresses there, thus reducing lateral friction.
- (2) Ideally, one model should correspond to one given value for the fluid pressure, cover thickness, and length of the sliding mass. Testing each parameter rapidly would amount to several tens of experiments, if not more. As construction and deformation of each model took several days, we had to limit the total number of experiments for logistical reasons and therefore, could not undertake several tens of experiments. To compensate for this limitation, we progressively varied the value of one parameter (namely, the applied pore-fluid pressure) during the experiment, assuming that this single experiment represented several experiments conducted under different air-pressure values. This approach worked very well with incised models. In these

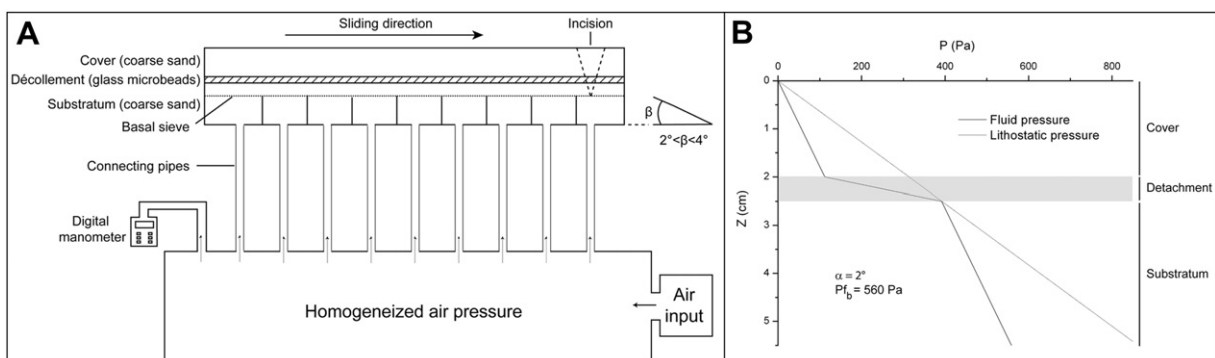


Fig. 5. Experimental setup. A: Schematic cross-section view. B: Theoretical pressure profiles within the model. α is the basal slope angle, Pf_b is the applied basal fluid pressure. Note that the fluid pressure approaches the lithostatic pressure at the base of the microbeads layer.

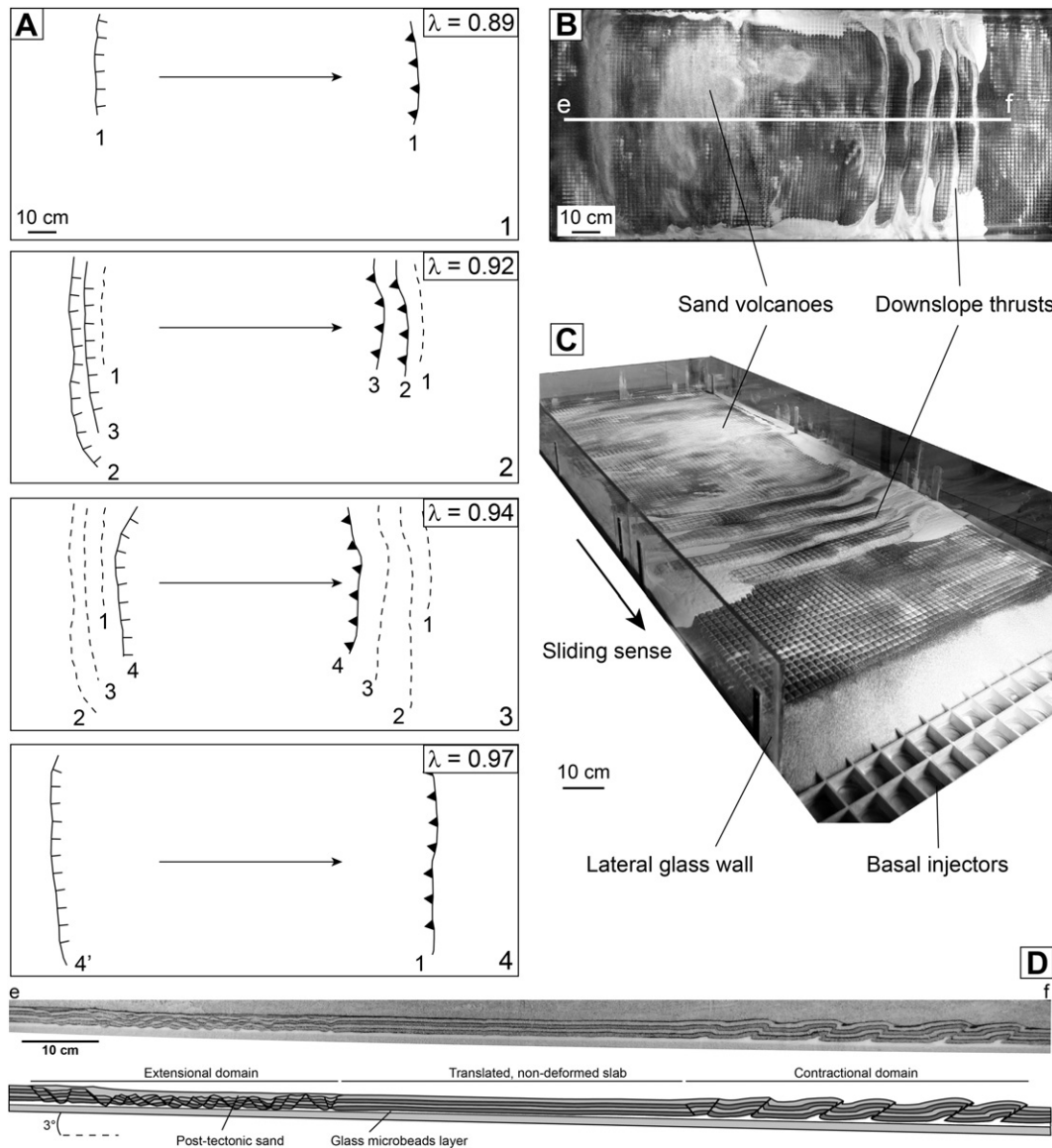


Fig. 6. Structural evolution of the buttressed models, example of a model having a 2 cm-thick cover and a 3° basal slope angle. A: Line drawings of the evolution of deformation, from the first stage (1) to the last stage (4) of deformation, with increasing λ_b . Numbers indicate the order of formation of the upslope normal faults and the related downslope thrusts. B: Overhead photograph of the ultimate stage of deformation. C: 3-D view of the ultimate stage of a buttressed model. D: Cross section (up) and line drawing (bottom). See (B) for location. The arrows indicate the sense of sliding.

models, the analytical solution predicts a *maximum* value of the slid mass length, and this value *increases* with *increasing* applied fluid pressure. Thus, during one single experiment, the first slide was short (providing the critical value for the slid mass under low fluid pressure conditions), then, as air pressure increased, the slid length increased, indicating the critical value for the slid mass for higher fluid pressure conditions (Lacoste et al., 2011). Consequently, one single experiment could be regarded as equivalent of a set of different experiments conducted under different values of pore-fluid pressure. Such an analogy is less straightforward when dealing with buttressed experiments, where the analytical model predicts a *minimum* critical length of the slid mass (i.e., longer block could also slide) that *decreases* with *increasing* fluid pressure (Mourgues et al., 2009).

Theoretically, testing this set up would need multiple models, each one having a given cover thickness and slope value, and a minimum area where the air pressure was applied, and check

whether sliding could occur. Then we would increase the area subjected to air pressure until sliding occurred. Such a scheme would have required hundreds of experiments. Instead, we ran models whose entire base was subjected to air pressure from the start, and progressively raised the air pressure as the model evolved. For specific critical values for cover thickness, basal slope, and fluid pressure, the model would deform. But if the length of the area subjected to air pressure was greater than the critical minimum value for sliding, the entire model was likely to slide. In other words, model results did not provide us with the value of this critical length, but a value that was – generally – greater than the critical one. We worked around this caveat by progressively increasing the air pressure in the model as it evolved. Typically, a long panel of the cover slid during the first episode, forming an array of normal faults updip and thrust faults downdip. Measuring the shortest distance between the two deformation domains provided the value for the length of the slid mass. With ongoing deformation and increasing fluid pressure, thrusts propagated

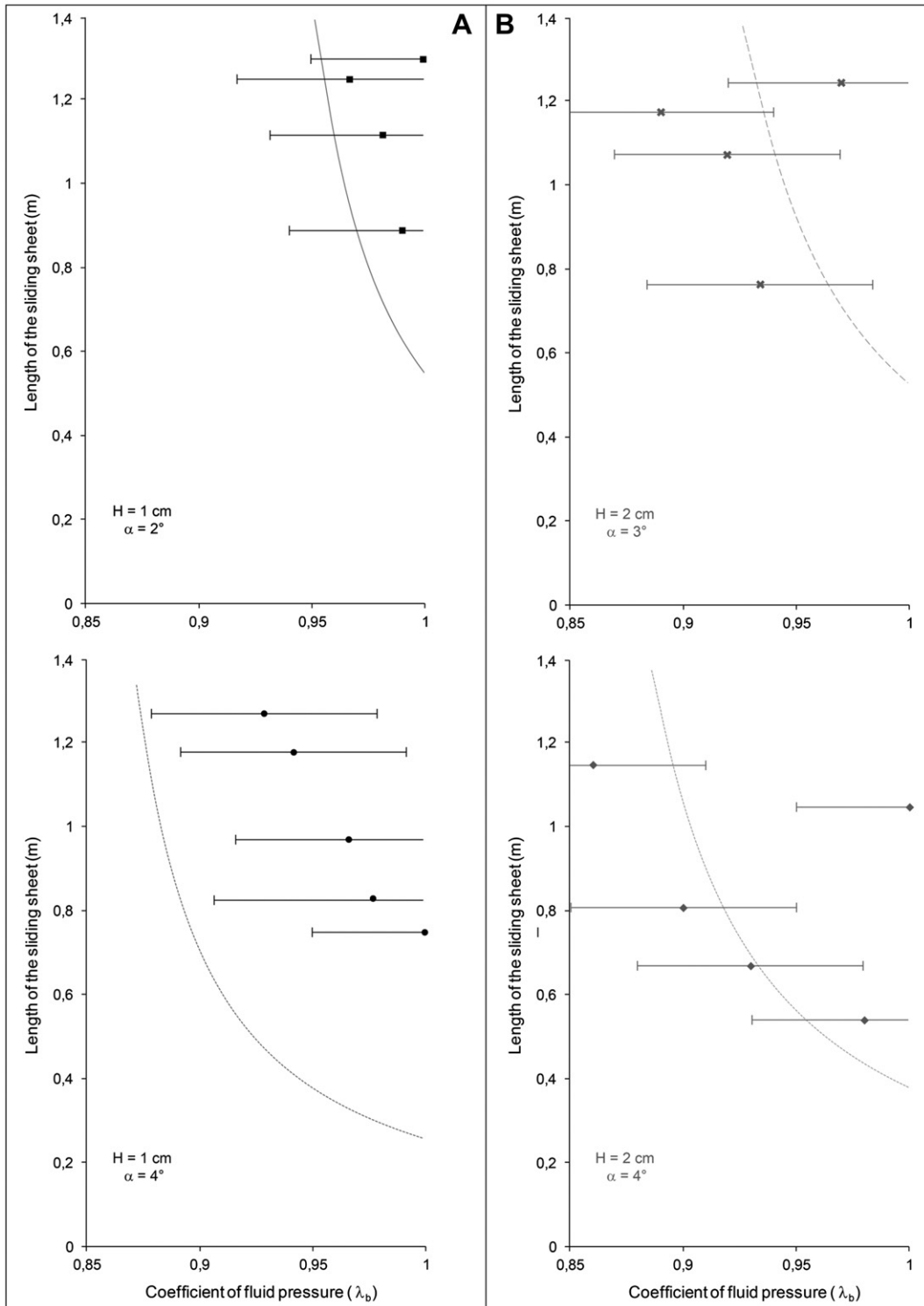


Fig. 7. Experimental evolutions of the sliding sheet length with respect to λ_b in buttressed models.

updip, while the extensional domain was passively translated downdip: the length of the cover block translated rigidly decreased until a point when the system became totally blocked, regardless of the air pressure we applied. At that stage, the length of the slid mass could be considered as the minimum critical length for a given cover-thickness/fluid-pressure configuration. So, unlike the non-buttressed experiments, each buttressed model could provide only one critical value and could not be regarded as a substitute for

multiple experiments. Moreover, the evolution of buttressed models also hindered the reliability of the procedure. During the early stages, where the length of the slid mass was usually greater than the critical length, thrusts and folds formed downdip, thickening the cover and the décollement, and normal faults formed updip where syntectonic sedimentation maintained the cover thickness constant, but the décollement thickness decreased. Overall, the conditions changed along the downslope and upslope

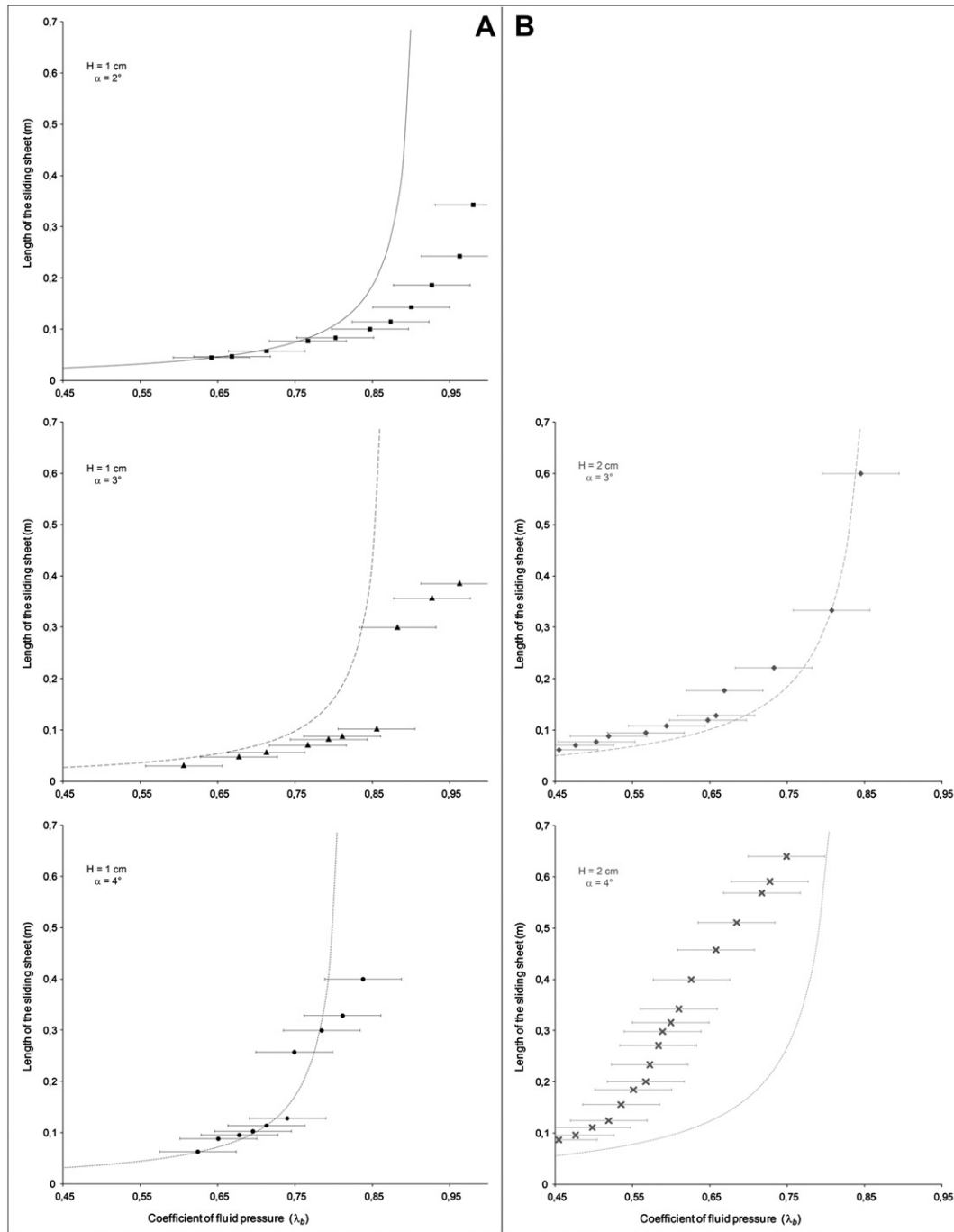


Fig. 8. Experimental evolutions of the sliding sheet length with respect to λ_b in incised models.

boundaries of the system, and this change may have had some influence on the result. These observations explain why the quantitative data collected on the buttressed models are a bit more erratic in matching the solutions predicted by the analytical model.

3.3. Results

Each experiment was conducted twice to ensure that the results were reproducible. We measured the average values of the sliding sheet lengths, with respect to the coefficient of fluid pressure (λ_b) calculated at the base of the low-permeability microbeads layer, for cover thicknesses of 1 cm and 2 cm, and basal slope angles ranging from 2° to 4° . We estimated the error in the determination of the

coefficient of fluid pressure to be ± 0.05 . This estimation accounts for the precision of the digital manometer and uncertainties in the permeability values of the materials, which are difficult to evaluate and can also vary depending on the way in which the different layers were deposited. The models with basal slope angles lower than 2° are not presented here because sand volcanoes formed and the models eventually blew out before the experiments ended.

3.3.1. Buttressed models

As observed by Mourgues and Cobbold (2006) and Mourgues et al. (2009), the slid mass comprised three domains (Fig. 6). An extensional domain formed first on upper edges of the models. A translated, non-deformed slab has been observed at mid-slope.

Contractional structures developed on lower edges (Fig. 6A₁) and, with air pressure increasing, propagated updip (Fig. 6A_{2–3}). When the air pressure reached large values, such as models having a 2 cm cover thickness and a 3° basal slope angle, $\lambda_b = 0.97$, the model slid as a whole (Fig. 6A₄). This deformation stage reused the first formed thrust. Thickening of the downslope contractional toe eventually blocked deformation propagation. With increasing air pressure, sand volcanoes formed (Fig. 6B and C). These volcanoes appeared first on or near normal faults, where faulting had thinned the cover, thereby decreasing the lithostatic pressure and increasing the coefficient of fluid pressure.

In the buttressed models, the sliding sheet lengths decreased with increasing λ_b (Fig. 7). The sliding sheet length increase where the coefficient of fluid pressure reached values close to $\lambda_b = 1$ (Fig. 7) was due to changes in boundary conditions caused by the formation of successive thrusts and the thickening of the lower edge of the models (see Section 5.2).

3.3.2. Incised models

The sliding sheet lengths in incised models increased with λ_b increasing (Fig. 8). We observed a threshold in λ_b , above which the length of the sliding sheet greatly increased. This threshold was better expressed in the models having the thinner cover (thickness = 1 cm) than in the models having a 2 cm-thick cover. In the latter case, sliding sheet lengths evolved exponentially, without clearly defining any threshold. As in the theoretical predictions (Fig. 4B), an increase in cover thickness and/or in the basal slope angle reduced the value of the coefficient of fluid pressure required for the cover to slide (Fig. 8). For example, in the case of a 1 cm-thick cover, in order for the slide to reach a length of 30 cm, λ_b must be equal to 0.97 where the system is tilted by 2°, 0.88 where it is tilted by 3°, and 0.78 where it is tilted by 4° (Fig. 8).

4. Discussion

4.1. Sliding processes in models subjected to fluid overpressure

Numerous experiments have emphasized the role of pore-fluid pressure in the triggering of mass movements (e.g., Wang and Sassa, 2003; Mourgues et al., 2009; Lacoste et al., 2011). However, an important distinction should be made between the influence of fluid overpressure *in the cover* and *along the base* of the cover, respectively. On one hand, slope instability arises from water flows (Ghassian and Ghareh, 2008) and saturation of the potentially mobile cover (Wang and Sassa, 2003). In that case, sliding takes place on or near the top of the basal detachment layer (e.g., swelling clays, Shuzui, 2001). On the other hand, the critical decrease in the effective stress along the base of an overpressured layer allows for sliding of the overlying cover to occur, regardless of the fluid saturation of this cover.

Our results confirm that, in models having a downslope buttress, the sliding sheet length decreases with the basal pore-fluid pressure increasing, as observed by Mourgues and Cobbold (2006) and Mourgues et al. (2009). In these models, the contractional structures form first in the downslope part and propagate updip. This stacking mechanism is similar to that described in experimental salt-detached gravity-driven thrusts belts by Dooley et al. (2007). In contrast, in models subjected to downslope incision, the sliding sheet length increases with increasing pore-fluid pressure.

The presence of a downslope resisting force prevents the formation of slope instability below a threshold of the coefficient of fluid pressure (λ_b) (Figs. 3 and 7), for which the value of the frictional resisting force at the base of the cover decreases enough to allow for sliding to occur. In buttressed models where the value of

λ_b was smaller, the driving forces induced by the weight of the cover and/or the basal slope had to reach sufficient values to overcome the buttressing resistance (Fig. 7). An increase in cover thickness, basal slope angle and/or coefficient of fluid pressure causes a decrease in the sliding sheet length, i.e., the distance between the upslope normal fault and the downslope thrust (Fig. 6; Mourgues and Cobbold, 2006).

In incised models subjected to fluid overpressure, combined low basal resistance related to fluid overpressure and the lack of downslope buttress critically reduce the forces resisting sliding and trigger deformation, even where the driving forces are moderate. In such a case, slope instabilities can form even at small λ_b values (Figs. 4B and 8). The driving forces F_w and F_σ do not depend on the coefficient of fluid pressure. Therefore, with λ_b increasing, the sliding sheet lengths increase (Fig. 8), because of the progressive decrease in the value of the frictional force F_b . In the absence of distal buttress, the deformation thus propagates retrogressively from the valley flanks upslope (Lacoste et al., 2011). To limit the total number of experiments, we decided to raise the air pressure progressively. Nonetheless, with the coefficient of fluid pressure remaining constant, an increase in the basal slope (i.e., the driving forces F_w and F_σ) would have yielded similar results.

The mechanical behaviour of the material during the deformation phases may also affect the geometry and kinematics of the sliding masses. Early studies showed that deformation had a strong influence on the mechanical properties of natural rocks (Byerlee, 1978; Paterson, 1978). Following these observations, Lohrmann et al. (2003) demonstrated that granular analogue materials were subjected to strain hardening prior to failure and subsequent strain softening. This transition from peak strength to residual strength during deformation could account for the structural evolution of the slides. However, Schreurs et al. (2006) showed that the glass microbeads used in our experiments (Table 1) are subjected to <9% strain softening, which represents a change between peak and residual angle of internal friction <2°. This effect is therefore negligible in comparison with the influence of increasing air pressure on the reduction of the basal frictional resisting force.

4.2. Comparison between experimental and analytical models

The experimental results are in good agreement with the theoretical predictions of the analytical model. The predicted evolutions of the sliding sheet lengths are depicted in the models by the propagation of the extensional and contractional domains. In models having a downslope buttress, we observed an exponential decrease in the sliding sheet length with increasing λ_b , except in the experimental model having a 2 cm-cover thickness and a 2°-basal slope angle (not presented in this article), in which this decrease was moderate. In the latter model, strong lateral friction combined with weak driving forces hampered sliding. In models subjected to incision, the sliding sheet length increased exponentially with increasing λ_b . We also observed that the coefficient of fluid pressure required for the cover to slide decreased with the basal slope angle and/or the cover thickness increasing (Figs. 4B and 8). An increase in the cover thickness also decreases the concavity of the curve (Fig. 4B). In the analogue models, the sliding lengths evolutions in models having a 2 cm-thick cover effectively tend to be more linear.

However, despite the general agreement between the analytical and experimental curves, several differences require further discussion. No vertical asymptote, corresponding to the infinite-slope model case (Crans et al., 1980; Mello and Pratson, 1999), was observed in our analogue models. Indeed, the evolution of deformation in the experiments led to different stress states than the initial boundary conditions, for which the analytical curves were drawn. In the buttressed models case, the calculated sliding

length is a minimum length. In the experiments, the slides may have a length greater than that minimum value (Fig. 6A₄). The progressive thickening of the cover increased the resisting force at the base of the slope, which favoured the updip propagation of the deformation during the first episodes of sliding. However, in late stages (Fig. 6A₄), the buttressing force reached a critical value and prevented the formation of new structures, therefore leading to the resumption of motion along former thrusts. As a consequence, in buttressed models, the measured sheet length is not always the minimum sliding length (see Section 4.2). This difference could account for discrepancies between the analytical and analogue models.

In the incised models case, the thinning of the cover and the important amount of strain at the base of the slope at the end of experiments hampered sliding of infinitely-long sheets, as predicted by the analytical calculations (infinite slope model, Crans et al., 1980; Mello and Pratson, 1999). Moreover, in these experiments, we simulated river incision by vacuuming the downslope part of the cover. The valley flank slope was controlled by the angle of repose of the cohesionless sand (34°, Table 1). In practice, the downslope wedge-like geometry of the cover generated a resisting force. As weak a force as this might be, it turned out to be great enough to prevent the whole cover from sliding. In the experiments with incision that involved a 2 cm-thick cover, the sharp increase in the sliding-sheet length with increasing λ_b was not clearly visible, except for the 3°-basal slope angle model (Fig. 8). Because the resisting force induced by the wedge increases with increasing cover thickness, it therefore opposes sliding in the models having a thick cover (i.e., 2 cm), even where the frictional basal force (F_b) had been reduced by the effect of fluid overpressure.

Lateral friction along the sidewalls may also have a strong influence on sliding evolution by adding a supplementary resisting force. Because the driving forces as compared with forces generated by the sedimentary cover thickness and the basal slope angle, as well as the shear frictional resisting force at the base of the cover, are small, lateral frictional forces can become proportionally quite important, and control the evolution of deformation of analogue models subjected to fluid overpressure (Costa and Vendeville, 2004; Schreurs et al., 2006; Vendeville, 2007). Therefore, to overcome the resulting force resisting sliding, the driving forces (the basal slope angle and/or the cover thickness) must be increased.

The evolution of the sliding sheet length with respect to λ_b also depends on the values of the décollement layer and cover cohesion. High cohesion values hamper sliding. In our analytical calculations (Fig. 4), we assumed that our sands were dry and had no cohesion. However, air-moisture in the laboratory may have raised the sand's cohesion to non-negligible levels. The materials (sand and glass microbeads) that we used in these models could then have had a cohesion greater than previously expected when the experiments were performed, which would lead to greater resistance to sliding. Further experiments involving cohesive materials would be required to confirm this hypothesis.

5. Conclusions

We developed a 2-D analytical model that investigated the influence of incision and the removal of downslope buttress on the structural evolution of a cover sliding on a low-permeability layer subjected to fluid overpressure. We also conducted analogue experiments that helped us better understand the style and evolution of deformation determined with the analytical calculations. Model results show that sliding deformation processes greatly differ depending on whether a distal buttress is present or not:

- In models having a downslope buttress, the sliding sheet length decreases with the coefficient of fluid pressure (λ_b) applied at the base of the model increasing.
- In models subjected to downslope incision, the sliding sheet length increases with λ_b increasing. Slope instabilities may form even in the case when values of λ_b are low.
- In both buttressed and incised models, the value of λ_b required for the cover to slide decreases when the basal slope angle and/or the cover thickness increase (albeit with less impact than the slope angle).
- Deformation in incised models is controlled by extensional structures spreading retrogressively from the valley flank upslope. In buttressed models, deformation is mostly accommodated by contractional structures forming on the lower edges of the models. These structures migrate updip as the basal pore-fluid pressure is increasing.

Acknowledgments

We are grateful to José Miguel Azañón and Michel Jaboyedoff for careful and constructive reviews.

Appendix

A.1. Balance of forces in a frontally confined system

On a segment of a cohesionless system defined between an extensional part upslope and a thrust front downslope (Fig. A1), the balance of forces along the x -axis can be written as:

$$F_w + F_\sigma + F_b = 0 \quad (\text{a1})$$

where F_w is the x -component of a gravitational body force expressed with the buoyant weight:

$$F_w = \rho_e g H L \sin \alpha \quad (\text{a2})$$

with L , the length of the sliding sheet and H its thickness. F_b is the surface force exerted at the base and governed by the frictional sliding condition (6). Assuming no lateral variation of frictional resistance along the décollement, we can write:

$$F_b = \int_L \tau_b dx = -\mu_b \sigma'_{zz} = -\mu_b (1 - \lambda_b) \rho_e g H L \cos \alpha \quad (\text{a3})$$

F_σ is the net force exerted by σ'_{xx} acting on the upper and lower edges of the system (Fig. A1):

$$F_\sigma = F_\sigma^{\text{ext}} - F_\sigma^{\text{toe}} = \int_H \sigma'_{xx}{}^{\text{ext}} b dh - \int_H \sigma'_{xx}{}^{\text{toe}} b dh \quad (\text{a4})$$

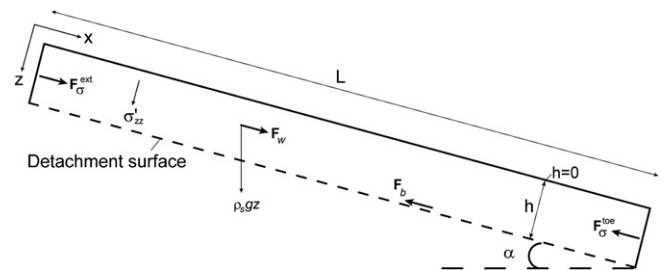


Fig. A1. Stresses and forces applied in our model. F_w is the driving force induced by the weight of the model, F_b is the basal frictional resisting force, F_σ^{ext} and F_σ^{toe} are the forces exerted by σ'_{xx} acting on the upper and lower edges of the system, respectively.

When the system starts sliding, normal faults form at the upper edge and thrust faults appear at the lower edge, as postulated by Nye (1952) in the case of glacier deformation. σ'_{xx} in both edges may thus be calculated at yield. In the extensional part, Mandl and Crans (1981) calculated that the dips of the normal faults depend on the amount of fluid overpressure in the cover. Mourgues and Cobbold (2003) used sandbox experiments to verify these predictions and noted that the orientation of the main principal stress was influenced by the seepage force, a force assumed to be perpendicular to the slope. They also showed that the dips of the normal faults could be described by using expressions of σ'_{xz} and σ'_{zz} deduced from the infinite slope model:

$$\sigma'_{xz} = \rho_e g z \sin \alpha \quad (\text{a5})$$

$$\sigma'_{zz} = (1 - \lambda) \rho_e g z \cos \alpha \quad (\text{a5.1})$$

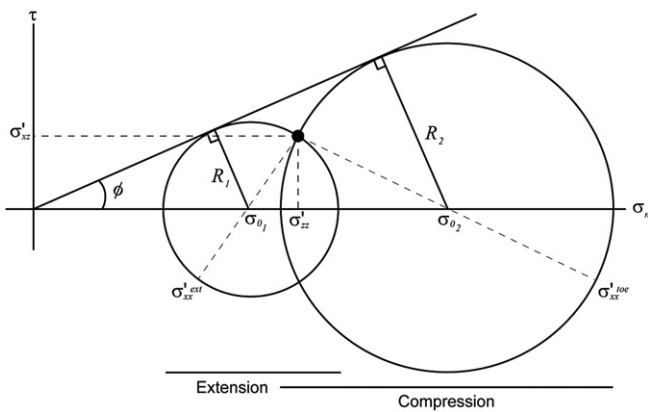


Fig. A2. Mohr's circle representation of the values of σ'_{xx} in the upslope part ($\sigma'_{xx}^{\text{ext}}$, extension) and downslope part ($\sigma'_{xx}^{\text{toe}}$, compression) of the model.

We used this hypothesis to estimate σ'_{xx} in the extensional trailing edge ($\sigma'_{xx}^{\text{ext}}$) and in the contractional leading edge ($\sigma'_{xx}^{\text{toe}}$). The associated extensional and contractional states of stress correspond to Rankine active and passive states, respectively (Lambe and Whitman, 1969). Fig. A2 shows the Mohr circle for this state of stresses, according to hypotheses (a5) and (a5.1), assuming no cohesion. From simple geometrical considerations (Fig. A2), we can write:

$$r = \sigma_0 \sin \phi = \sqrt{\sigma'_{xz}{}^2 + ((\sigma'_{xx} + \sigma'_{zz})/2)^2} \quad (\text{a6})$$

$$\sigma_0 = (\sigma'_{xx} + \sigma'_{zz})/2 \quad (\text{a7})$$

Combining Eqs. (a5.1)–(a7), we find:

$$\sigma'_{xx} = \sigma'_{zz}(2Y - 1) \quad (\text{a8})$$

with $Y = (1 \pm \sin \phi \sqrt{1 - \text{FS}^2})/\cos^2 \phi$. FS can be considered as a factor of safety evaluating the internal stability of the cohesionless cover:

$$\text{FS} = \tan \alpha / ((1 - \lambda) \tan \phi) \quad (\text{a9})$$

The sedimentary cover becomes unstable for $\text{FS} \geq 1$. F_σ can be evaluated from Eq. (a4):

$$F_\sigma = -2(1 - \lambda) \mu \rho g H^2 \frac{\cos \alpha}{\cos \phi} \sqrt{1 - \text{FS}^2} \quad (\text{a10})$$

The length of the sliding sheet can then be calculated:

$$L = \frac{2(1 - \lambda) \mu \sqrt{1 - \text{FS}^2}}{(\tan \alpha - (1 - \lambda_b) \mu_b) \cos \phi} H \quad (\text{a11})$$

The negative value of F_σ in Eq. (a10) shows this force acts as a resisting force. Therefore, sliding only occurs if the condition $(1 - \lambda_b) \mu_b \leq \tan \alpha$ is satisfied. Where $(1 - \lambda_b) \mu_b = \tan \alpha$, L reaches an infinite length. This limit corresponds to the infinite slope model and is satisfied for $F_\sigma = 0$. Beyond this limit, as the pore fluid pressure λ_b increases, the length of the sliding sheet allowed to glide decreases.

A.2. Length of a sliding sheet where the distal buttress is absent

In comparison with the buttressed model, the seepage force now has an x-component that must be added to the balance of forces. Eq. (a1) then becomes:

$$F_W + F_\sigma + F_b + F_{\text{SF}} = 0 \quad (\text{a12})$$

F_{SF} is the x-component of the seepage force:

$$\begin{aligned} F_{\text{SF}} &= - \int_V \int \vec{\nabla} P_{\text{OV}} dv = - \int_S \int P_{\text{OV}} \vec{dS} = \int_H P_{\text{OV}} dh \\ &= 0.5 \lambda \rho_e g H^2 \cos \alpha \end{aligned} \quad (\text{a13})$$

F_W can then be expressed as:

$$F_W = \rho_e g H L \sin \alpha + 0.5 \rho_e g H^2 L \sin \alpha / \tan \beta \quad (\text{a14})$$

where β is the angle of the downslope wedge and L the length of the slide. Assuming that σ'_{zz} may be estimated by Eq. (a5) along the detachment, the basal frictional force F_b becomes:

$$F_b = -\mu_b (1 - \lambda_b) \rho_e g H \cos \alpha (L + 0.5H / \tan \beta) \quad (\text{a15})$$

Combining Eqs. a12–a15, length L is given by:

$$L = 0.5 \left(\frac{(1 - \lambda)(2Y - 1) + \lambda}{\mu_b (1 - \lambda_b) - \tan \alpha} - \frac{1}{\tan \beta} \right) H \quad (\text{a16})$$

Unlike in the buttressed model case, sliding here occurs even if $(1 - \lambda_b) \mu_b \geq \tan \alpha$ is not satisfied yet. Indeed, in incised models, F_σ becomes a driving force ($F_\sigma > 0$) and a seepage force is added. L increases with λ_b . In other terms, deformation starts close to the downslope wedge and spreads retrogressively.

If the cover is cohesive, Eq. (a8) is modified as $\sigma'_{xx}^{\text{ext}}$ and z are not linearly dependent. The expression of F_σ^{ext} becomes more complex and must be numerically integrated. Close to the surface, σ'_{xx} becomes negative (Fig. A2). If cohesion is high enough, F_σ may even transform into a resisting force ($F_\sigma < 0$). In such a case, and for $F_\sigma + F_{\text{SF}} < 0$, sliding is only triggered for $(1 - \lambda_b) \mu_b \leq \tan \alpha$. This behaviour is similar to the behaviour of the buttressed model, where sliding starts with an infinite length.

References

- Azañon, J.M., Azor, A., Vicente Pérez-Peña, J., Carrillo, J.M., 2005. Late Quaternary large-scale rotational slides induced by river incision: the Arroyo de Gor area (Guadix basin, SE Spain). *Geomorphology* 69, 152–168.
- Byerlee, J., 1978. Friction of rocks. *Pure and Applied Geophysics* 116, 615–626.
- Chen, H., Dadson, S., Chi, Y.-G., 2006. Recent rainfall-induced landslides and debris flow in northern Taiwan. *Geomorphology* 77, 112–125.
- Cobbold, P.R., Mourgues, R., Boyd, K., 2004. Mechanism of thin-skinned detachment in the Amazon Fan: assessing the importance of fluid overpressure and hydrocarbon generation. *Marine and Petroleum Geology* 21, 1013–1025.
- Costa, E., Vendeville, B., 2004. Experimental insights on the geometry and kinematics of fold-and-thrust belts above weak, viscous evaporitic décollement: reply to comments by Hemin Koyi and James Cotton. *Journal of Structural Geology* 26, 2141–2143.

- Crans, W., Mandl, G., Haremboure, J., 1980. On the theory of growth faulting: a geomechanical delta model based on gravity sliding. *Journal of Petroleum Geology* 2, 265–307.
- Dahlen, F.A., 1984. Non-cohesive critical Coulomb wedges: an exact solution. *Journal of Geophysical Research* 89, 10125–10133.
- Dahlen, F.A., 1990. Critical taper model of fold-and-thrust belts and accretionary wedges. *Annual Review of Earth and Planetary Science* 18, 55–99.
- Davis, D., Suppe, J., Dahlen, F.A., 1983. Mechanics of fold-and-thrust belts and accretionary wedges. *Journal of Geophysical Research* 88 (B2), 1153–1172.
- Dooley, T.P., Jackson, M.P.A., Hudec, M.R., 2007. Initiation and growth of salt-based thrust belts on passive margins: results from physical models. *Basin Research* 19, 165–177.
- Ghiassian, H., Ghareh, S., 2008. Stability of sandy slopes under seepage conditions. *Landslides* 5, 397–406.
- Hafidason, H., Sejrup, H.P., Nygard, A., Mienert, J., Bryn, P., Lien, R., Forsberg, C.F., Berg, K., Masson, D., 2004. The Storegga Slide: architecture, geometry and slide-development. *Marine Geology* 213, 201–234.
- Hooper, R.J., Fitzsimmons, R.J., Grant, N., Vendeville, B.C., 2002. The role of deformation in controlling depositional patterns in the south-central Niger Delta, West Africa. *Journal of Structural Geology* 24, 847–859.
- Hubbert, M.K., Rubey, W.W., 1959. Role of fluid pressure in mechanics of overthrust faulting. *Geological Society of America Bulletin* 70, 115–166.
- Keefer, D.K., 1984. Landslides caused by earthquakes. *Geological Society of America Bulletin* 95, 406–421.
- Lacoste, A., Loncke, L., Chanier, F., Bailleul, J., Vendeville, B.C., Mahieux, G., 2009. Morphology and structure of a landslide complex in an active margin setting: the Waitawhiti complex, North Island, New Zealand. *Geomorphology* 109, 184–196.
- Lacoste, A., Vendeville, B.C., Loncke, L., 2011. Influence of combined incision and fluid overpressure on slope stability: experimental modelling and natural applications. *Journal of Structural Geology* 33, 731–742.
- Lambe, T.W., Whitman, R.V., 1969. *Soil Mechanics*. Wiley, New York, 553 pp.
- Lohrmann, J., Kukowski, N., Adam, J., Oncken, O., 2003. The impact of analogue material properties on the geometry, kinematics, and dynamics of convergent sand wedges. *Journal of Structural Geology* 25, 1691–1711.
- Mandl, G., 1988. Mechanics of tectonic faulting: models and basic concepts. In: *Developments in Structural Geology*. Elsevier, p. 407.
- Mandl, G., Crans, W., 1981. Gravitational gliding in deltas. In: McClay, K.R., Price, N.J. (Eds.), *Thrust and Nappe Tectonics*. Geological Society Special Publication, vol. 9, pp. 41–54.
- Mello, U.T., Pratson, L.F., 1999. Regional slope stability and slope-failure mechanics from the two-dimensional state of stress in an infinite slope. *Marine Geology* 154, 339–356.
- Mourgues, R., Cobbold, P.R., 2003. Some tectonic consequences of fluid overpressures and seepage forces as demonstrated by sandbox modelling. *Tectonophysics* 376, 75–97.
- Mourgues, R., Cobbold, P.R., 2006. Sandbox experiments on gravitational spreading and gliding in the presence of fluid overpressures. *Journal of Structural Geology* 28, 887–901.
- Mourgues, R., Lecomte, E., Vendeville, B., Raillard, S., 2009. An experimental investigation of gravity-driven shale tectonics in progradational delta. *Tectonophysics* 474, 643–656.
- Nye, J.F., 1952. The mechanics of glacier flow. *Journal of Glaciology* 2, 82–93.
- Panien, M., Schreurs, G., Pfiffner, A., 2006. Mechanical behaviour of granular materials used in analogue modelling: insights from grain characterisation, ring-shear tests and analogue experiments. *Journal of Structural Geology* 28, 1710–1724.
- Paterson, M.S., 1978. *Experimental Rock Deformation*. Springer, New York, 254 pp.
- Schellart, W.P., 2000. Shear test results for cohesion and friction coefficients for different granular materials: scaling implications for their usage in analogue modelling. *Tectonophysics* 324, 1–16.
- Schreurs, G., Buitier, S.J.H., Boutelier, D., Corti, G., Costa, E., Cruden, A.R., Daniel, J.-M., Hoth, S., Koyi, H.A., Kukowski, N., Lohrmann, J., Ravaglia, A., Schlische, R.W., Withjack, M.O., Yamada, Y., Cavozzi, C., Del Ventisette, C., Elder Brady, J.A., Hoffmann-Rothe, A., Mengus, J.-M., Montanari, D., Nilforoushan, F., 2006. Analogue benchmarks of shortening and extension experiments. In: *Geological Society of London Special Publication*, vol. 253, pp. 1–27.
- Shuzui, H., 2001. Process of slip-surface development and formation of slip-surface clay in landslides in tertiary volcanic rocks, Japan. *Engineering Geology* 61, 199–219.
- Terzaghi, K.v., 1923. Die Berechnung der Durchlässigkeitsziffer des Tones aus dem Verlauf der hydrodynamischen Spannungserscheinungen. *Akad. Wissensch. Wien, Math. Naturw. Kl. Abt. 132*, 125–138.
- Terzaghi, K.v., 1950. Mechanics of landslides. In: Paige, S. (Ed.), *Application of Geology to Engineering Practice*. Geological Society of America, pp. 83–123. New York.
- Terzaghi, K.v., 1959. Soil mechanics in action. *Civil Engineering* 29, 69–70.
- Van Rensbergen, P., Morley, C.K., 2000. 3D seismic study of a shale expulsion syncline at the base of the Champion delta, offshore Brunei, and its implications for the early structural evolution of large delta systems. *Marine and Petroleum Geology* 17, 861–872.
- Vendeville, B.C., 2007. The 3-D nature of stress fields in physical experiments and its impact on models overall evolution. In: *European Geosciences Union General Assembly*, 15–20 April.
- Wang, G., Sassa, K., 2003. Pore-pressure generation and movement of rainfall-induced landslides: effects of grain size and fine-particle content. *Engineering Geology* 69, 109–125.
- Weber, K.J., Daukoru, E.M., 1975. Petroleum geology of the Niger delta. In: *Proceedings of the Ninth World Petroleum Congress*. Geology, vol. 2. Applied Science Publishers, Ltd., London, pp. 210–221.
- Yamada, Y., Kaneda, K., Matsuoka, T., 2006. Influences of material properties on analogue model experiments of geologic structures. *Journal of the Society of Materials Sciences, Japan* 55, 452–457.